Prediction of plasticity-controlled failure in polyamide 6

Prediction of plasticity-controlled failure in polyamide 6: influence of temperature and relative humidity

E. Parodi[1,2], G. W. M. Peters[1,2], L. E. Govaert[1,2*]

[1] Department of Mechanical Engineering, Materials Technology Institute, Eindhoven University of Technology, P.O.Box 513, 5600 MB, Eindhoven, the Netherlands

[2] Dutch Polymer Institute (DPI), P.O. Box 902, 5600 AX Eindhoven, the Netherlands

*Author to whom correspondence should be addressed. E-mail: l.e.govaert@tue.nl Tel: +31 402472838

Abstract

In this study, the influence of temperature and relative humidity on the plasticity controlled failure of polyamide 6 was investigated. Uniaxial tensile tests (constant strain rate) are performed at several temperatures, strain rates and relative humidity; creep tests under constant load are instead performed at different relative humidity and applied load. In order to describe and predict the yield kinetics, the Ree-Eyring equation was used and modified in order to include the effect of relative humidity. Thus, employing the concept of critical plastic strain, the yield kinetics can be successfully translated to prediction of time-to-failure. A good agreement between predictions and experimental results is obtained, showing that the model is a suitable and versatile tool to predict mechanical properties of a temperature and moisture sensitive material as polyamide 6.

1 Introduction

Polyamide 6 is an engineering polymer commonly known as "Nylon 6"; it is one of the most used engineering polymers, which can be found in the form of fibers, films and also injection molded products. In the last decades it was also introduced in the field of load-bearing applications such as mechanical parts, under-hood components and sport items which are often exposed to demanding conditions combining high load, challenging temperature regimes and elevated relative humidities. These applications require a high level of reliability, thus an investigation of humidity and temperature influence on the mechanical properties is required. PA6 belongs to the family of aliphatic polyamides. Its monomer has two polar groups; the amide and carbonyl groups. These groups can form hydrogen bonds between chains, leading to high modulus and yield strength [1]. However, the polar character also causes a crucial issue of polyamide 6: hygroscopicity [2]. Indeed, if exposed to a humid environment, PA6 absorbs up to a saturation level which typically depends on temperature and relative humidity [3]. If this occurs, part of the hydrogen bonds are broken and new H bonds are formed with the absorbed water molecules [4]. This phenomenon leads to plasticization and results in a depression of the glass transition temperature [5] which also results in a considerable decrease of the mechanical properties [6, 7, 8, 9]. In case of exposure to humidity, T_g can drop to values lower than room temperature, in which case structural changes at room temperature may occur [10]. Another characteristic of PA6 is polymorphism; it can crystallize in (mainly) two forms, i) the most stable α-phase (monoclinic cell), which is obtained in low under-cooling or isothermal crystallization temperature higher than 170°C, and ii) the less stable γ-mesophase (pseudo-hexagonal cell) obtained at high under-cooling or isothermal crystallization at temperature between T_g and 170°C. In case of very fast cooling ($>$100°C/s) also a completely amorphous sample can be obtained [11].

Although lifetime prediction of polymers is a widely investigated topic, studies regarding PA6

neat are hardly found in literature [12, 13]. In general it is known that three different failure modes can be distinguished: a) plasticity controlled failure (high applied load), b) slow crack growth (medium load) and, c) molecular degradation (low or no load). The latter is regarded to be independent of applied stress, and is, at least in PA6, not regarded as a limiting factor. Crack growth controlled failure is mainly studied by cyclic fatigue [14, 15, 16], however it is a failure regime hardly achieved in the case of polyamide 6, due to its excellent fatigue properties. Finally, the plasticity controlled regime, where failure occurs by accumulation of plastic deformation, can be studied by uniaxial tensile test at constant applied strain rate and constant applied load (creep).

In this study, a model able to predict the plasticity controlled failure of polyamide 6 at different temperature and relative humidity is presented.

2 Background

Under constant load, solid polymers tend to display time dependent deformation (creep) and, ultimately failure occurs. A creep curve can be divided in three regimes: primary creep where the strain rate decreases in time, secondary creep in which strain rate remains constant, and tertiary creep where strain rate increases in time due to intrinsic or geometric softening and eventually failure occurs. The time-to-failure depends on the applied load and temperature, where an increase of these two leads to a decrease of time-to-failure, as shown in literature by [17, 18]. Important in lifetime prediction is an estimate of the plastic flow during secondary creep. Bauwens-Crowet *et al*. [19], has shown that the steady state reached at yield point in constant strain rate experiment is the same of the one reached in the secondary creep. Thus, stress- and temperature-dependence measured in constant strain rate experiments can be used to describe the kinetics of plastic flow. The deformation kinetics are described by the Eyring's

activated flow theory [20]:

$$\dot{\varepsilon}_{pl}(\sigma,T) = \dot{\varepsilon}_0 \; exp\left(-\frac{\Delta U}{RT}\right) \; sinh\left(\frac{\sigma V^*}{kT}\right) \tag{1}$$

where $\dot{\varepsilon}_0$ is a rate factor, σ is the yield stress, V^* is the activation volume, ΔU is the activation energy, R is the universal gas constant, k is the Boltzmann's constant and $T$the absolute temperature.

Plotting the plastic flow rate for each applied load as a function of the corresponding time-to-failure, a linear relation with slope -1 (in a double logarithmic plot) is found [21], this implies that the product of $\dot{\varepsilon}_{pl}$ and t_f is constant:

$$\dot{\varepsilon}_{pl}(\sigma)\cdot t_f(\sigma) = C \tag{2}$$

The constant C, mentioned in equation 2, can be defined as critical strain, ε_{cr}, which equals the accumulated plastic strain for a material subjected to the plastic flow rate, $\dot{\varepsilon}_{pl}$. By this phenomenological approach and by the stress- temperature-dependence of the plastic flow rate, the prediction of time-to-failure under a constant load is achieved:

$$t_f(\sigma,T) = \frac{\varepsilon_{cr}}{\dot{\varepsilon}_{pl}(\sigma,T)} \tag{3}$$

In order to determine the stress- and temperature-dependence of plastic flow rate, constant strain rate experiments are the most suitable because of their low time consumption and planning possibilities. In a stress strain response curve obtained by tensile test the first part (at low strain) is the elastic region, in which chain mobility is negligible and the elastic modulus depends on intermolecular interactions among chains; when strain achieves a certain level, changes in chain conformation take place and plastic deformation occurs; increasing the strain even further, mobility increases with stress until a point in which it matches the applied strain rate, this point is called yield stress. In order to strain a solid polymer at higher strain rate, higher stress is required to induce higher mobility [22].

3 Experimental

3.1 Materials

The material employed in this work was a polyamide 6 (Akulon K122) kindly provided by DSM (The Netherlands). This PA6 has a viscosity average molar mass (Mv) of about 24.9 kg/mol.

3.2 Sample preparation

Sheets with a thickness of 0.5mm were prepared by compression molding. After a careful drying procedure (1 night at 110°C under vacuum) the pellets were placed in a "sandwich" consisting of two thick steel plates (about 3mm), two thin aluminum foils (about 0.2mm) and a 250×250×0.5mm steel mold. The material was melted at 265°C for 5 minutes, while a force of about 10kN was applied. Then, the "sandwich" was rapidly moved to a cold press set at 80°C where the material was solidified in quiescent condition for 3 minutes. According to the ISO527 type 1BA, dog-bone samples were prepared using a cutting die (main measures: width 5mm, length 22mm).

3.3 Sample conditioning

In order to investigate the influence of hydration, samples were stored at four different relative humidities, RH0% (dry), RH35%, RH50% and RH75%. In the case of dry conditioning, samples were stored in a desiccators under vacuum at room temperature; for RH50% an environmental chamber was employed. While in the case of RH35% and RH75% two desiccators, containing supersaturated salt solutions able to maintain a constant relative humidity in a close environment, were used. The salts were sodium chloride and magnesium chloride hexahydrate for 75 and 35% respectively.

3.4 Mechanical tests

Uniaxial tensile tests and creep tests under constant load were performed using a Zwick Z010 Unviversal Testing Machine equipped with a 1kN load-cell. The testing area is surrounded by an environmental chamber which allows to test at controlled temperature and humidity. The tensile tests were performed, at least in duplicates, in a range of strain rates from $10^{-5}\ s^{-1}$ up to $3{\cdot}10^{-2}\ s^{-1}$, temperatures between -40°C and 120°C (in dry condition) and relative humidity of 35, 50 and 75% (at room temperature). Before starting the experiments, a pre-load of 0.1 MPa was applied at a speed of 1mm/min. Creep measurements were performed at relative humidity of 35, 50, and 75%. The stress was applied within 10 seconds and subsequently kept constant until failure. The time-to-failure was estimated as the time at which the strain reaches the value of 25%, which was defined as stain at failure. The plastic flow rate ($\dot{\varepsilon}_{pl}$) was estimated as the minimum in the Sherby-Dorn plot [23].

3.5 X-ray diffraction

Wide angle x-ray diffraction was performed at the European Synchrotron Radiation Facility in Grenoble (FR) at the Dutch-Belgian beamline (DUBBLE). After normalization, the crystallinity was estimated by subtracting an amorphous halo (experimentally obtained) to the measured patterns. The degree of crystallinity is finally calculated by:

$$\chi_c = \frac{A + C}{C} \tag{4}$$

where C is the total scattered intensity and A is the scattering from the amorphous halo. In order to estimate the effect of different conditioning on the crystallographic structures, a deconvolution analysis was performed. This was obtained by fitting Lorentzian functions, in proximity of each characteristic reflection. Eventually, all the Lorentzian functions and the amorphous halo were summed to verify the fidelity of the fitting procedure (green markers in

figure 1). Thus, the relative quantities $\chi_{c,\alpha}$ and $\chi_{c,\gamma}$ were calculated by the following:

$$\chi_{c,\alpha} = (\frac{A_l - A_\gamma}{A_m}) \qquad and \qquad \chi_{c,\gamma} = (\frac{A_l - A_\alpha}{A_m}) \tag{5}$$

where A_α and A_γ are the total area of the Lorentzian functions for the α and γ peaks, A_m is the total area of the measured pattern, and A_l is the sum off all the Lorentzian functions (α and γ). An example is given in figure 1.

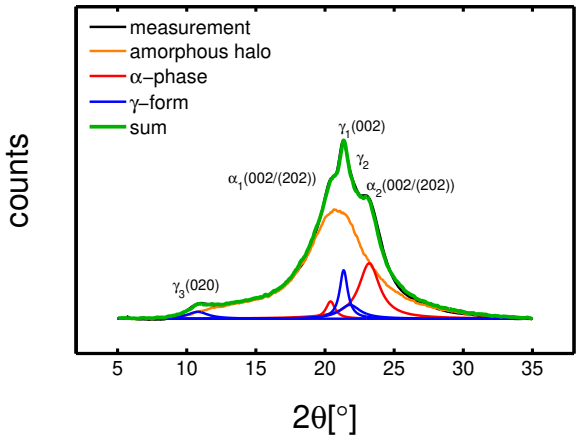

Figure 1: Example of WAXD pattern deconvolution analysis. The green line is the result of the deconvolution procedure, the orange line is the measured amorphous halo, blue and red curves are the Lorentzian functions.

3.6 Dynamical mechanical thermal analysis

In order to measure the glass transition temperature before and after conditioning, dynamical mechanical thermal analysis (DMTA) was performed by a TA instruments Q800 DMA. Samples were rectangular bars of about 5mm width, 0.5mm thickness. The experiments were carried out at a single frequency of 1Hz and along a temperature ramp from -40°C to 100°C with a heating rate of 3°C/min. The glass transition temperature was defined as the maximum in log $\tan(\delta)$.

4 Results and discussion

The first step of this investigation was a crystallographic characterization performed by wide angle x-ray diffraction experiments. These were carried out on the dry samples at room temperature; in figure 2a a 2D image is shown, as expected, the pattern is isotropic. In figure 2b, the result of a radial integration is given. The pattern shows the characteristics of γ-form, i.e. the main peak at about 2θ 21°, and the secondary peak at about 2θ 10°. By deconvolution analysis, the crystallinity was estimated to be around 30%.

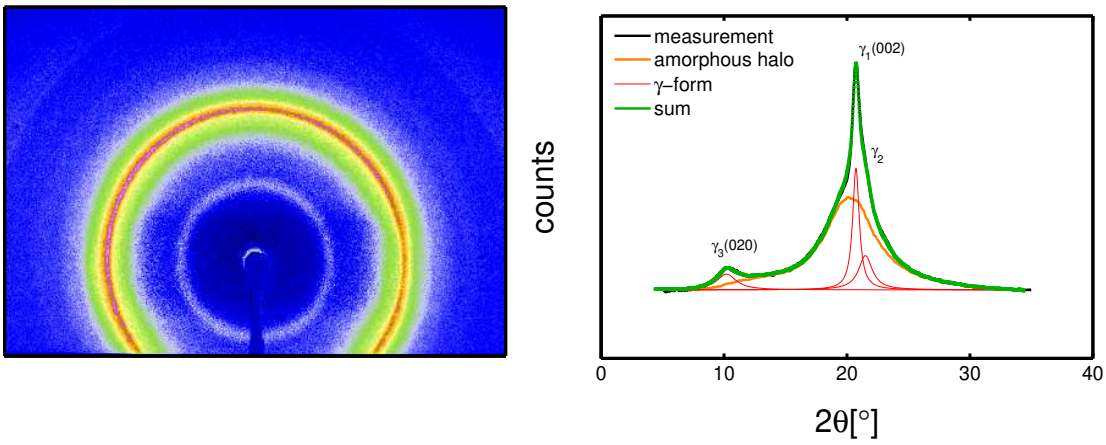

(a) (b)

Figure 2: a) Two-dimensional pattern of wide angle x-ray; b) radial integration of WAXD with deconvolution analysis.

4.1 Yield kinetics - dry state

The mechanical characterization started with tensile tests at several temperatures in dry condition at strain rates ranging from $10^{-4}\ s^{-1}$ to $3{\cdot}10^{-2}$. In figure 3a and 3b, the stress-strain response of dry samples at several temperatures and strain rates is shown; as expected, an increase of strain rate results in an increase of yield stress. Figure 4a shows the yield stress as a function of strain rate for different testing temperatures, in the case of samples at the dry state.

It is possible to notice that the strain rate-dependence of yield stress shows two different slopes, suggesting that the deformation occurs through two different molecular deformation, as already proposed by several authors [24, 25, 26, 21]. These two processes are generally attributed to an intra-lamellar deformation for processes I (low slope) and inter-lamellar for the processes II (high slope) [27, 28, 22]. It is stated that the stress contributions are additive, therefore the equation 1 is re-written and a part is added:

$$\sigma_y(\dot{\varepsilon},T) = \frac{kT}{V_I^*}\ sinh^{-1}\left(\frac{\dot{\varepsilon}}{\dot{\varepsilon}_{0,I}}\ exp\left(\frac{\Delta U_I}{RT}\right)\right) + \frac{kT}{V_{II}^*}\ sinh^{-1}\left(\frac{\dot{\varepsilon}}{\dot{\varepsilon}_{0,II}}\ exp\left(\frac{\Delta U_{II}}{RT}\right)\right) \tag{6}$$

where $\dot{\varepsilon}_{0,I}$, ΔU_I and V_I^* are rate factor, activation energy and activation volume related to process I and $\dot{\varepsilon}_{0,II}$, ΔU_{II} and V_{II}^* are related to the process II. In order to describe the results shown in figure 4a, the set of parameters shown in table 1 was employed.

Table 1: Eyring parameters.

	$V^*\ [m^3]$	$\Delta U\ [Jmol^1]$	$\dot{\varepsilon}_0\ [s^{-1}]$
I	$9{\cdot}e{-}27$	$1{\cdot}e6$	$1{\cdot}e123$
II	$1.9{\cdot}e{-}27$	$3{\cdot}e5$	$2{\cdot}e45$

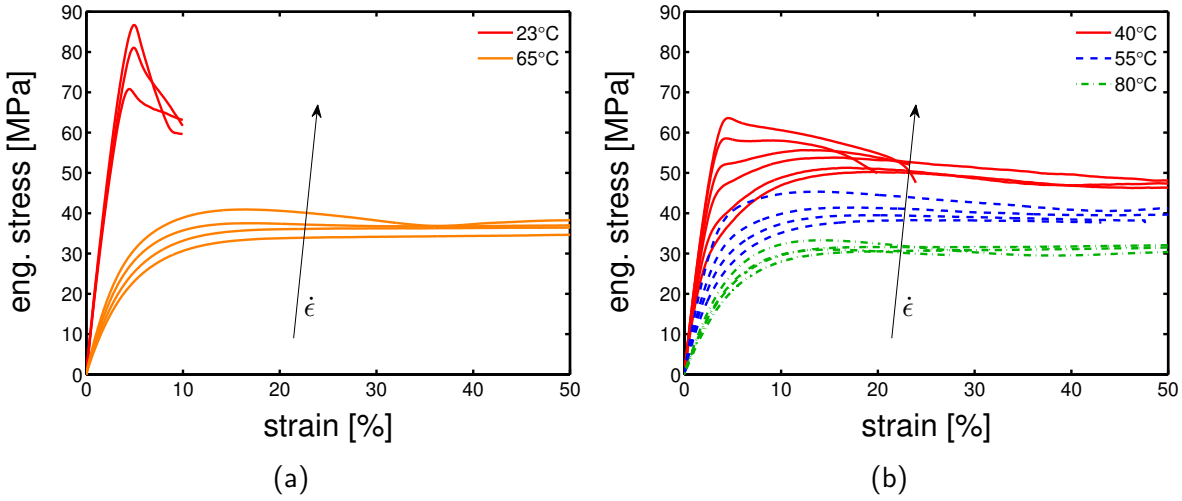

Figure 3: Stress-stain response of uniaxial tensile tests at a) 23, 65°C and b) 40, 55 and 80°C.

Finally, in figure 4b the yield kinetics of polyamide 6 at dry state is shown, in this case the lines are results of equation 6.

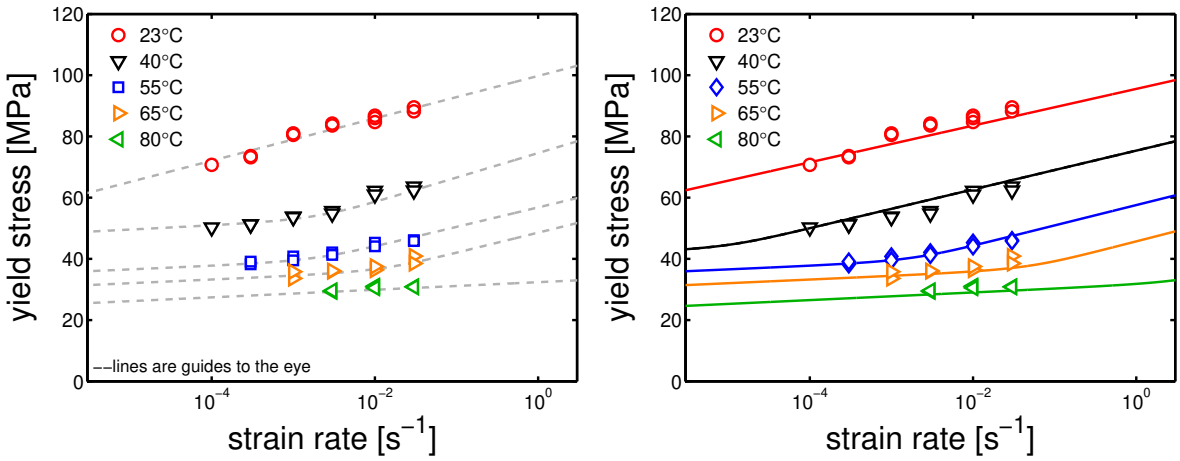

Figure 4: a) Yield kinetics of samples tested at different temperature at the dry state, lines are guides to the eye. b) Yield kinetics of polyamide 6 at dry state, the lines are results of equation 6 with parameter shown in table 1.

To further explore the kinetics, the stress-strain response was also investigated in a wide range of temperatures, from -40°C to 120°C, as shown in figure 5a. In figure 5b the yield stress is plotted as a function of temperature, the line is the result of equation 6 in the case of a fixed strain rate ($10^{-2}\ s^{-1}$) and a vector of temperatures. As shown, the model describe the results well in the range of temperature between 23°C and 100°C; as far as the description at low temperature is concerned, the deviation from the prediction is due to a geometrical effect. This is due to stress localization which takes place while stretching the sample beyond yield. It is visible also in figure 5a, in which it is possible to notice that the strain at yield sensibly shifts towards lower strain when the temperature decrease below 23°C. In appendix A examples of compression tests are given; in this case, the localization does not occur, thus the prediction results in good agreement with the results. At very high temperature (T>100°C), the temperature-dependence of yield stress flattens; this is due to an evolution of the crys-

tallographic structure during the test. In fact, at high temperature, well above T_g, the chain mobility is higher and lamellar thickening and/or cold crystallization occur (this phenomenon will be called "annealing"); this lead to an increase of yield stress in time. An example of this effect is given in figure 6a, where the samples are tested at 110°C in a range of strain rates from $3{\cdot}10^{-4}\ s^{-1}$ up to $3{\cdot}10^{-2}\ s^{-1}$. Figure 6a shows that the yield stress increases for decreasing strain rate, which is possible only in case of structural evolution during the test. Annealing is a time- and temperature-dependent phenomenon, its effect increases with increasing temperature and/or exposure time; thus, during an experiment at low strain rate, where the exposure time is high, more annealing will occur and yield stress will increase. Moreover, to understand whether the stress plays a role in annealing kinetics, another kind of experiment was performed; tensile tests were performed at constant strain rate after conditioning the samples at 110°C for several different exposure time. In figure 6b yield stress is plotted as a function of exposure time; the increase of yield due to annealing starts only after about 10^4 seconds, while in the case of figure 6a, an increase of yield stress is visible already in the case of strain rate $10^{-2}\ s^{-1}$ which is equivalent to about 350 seconds (300 s without stress + 50 s with stress).

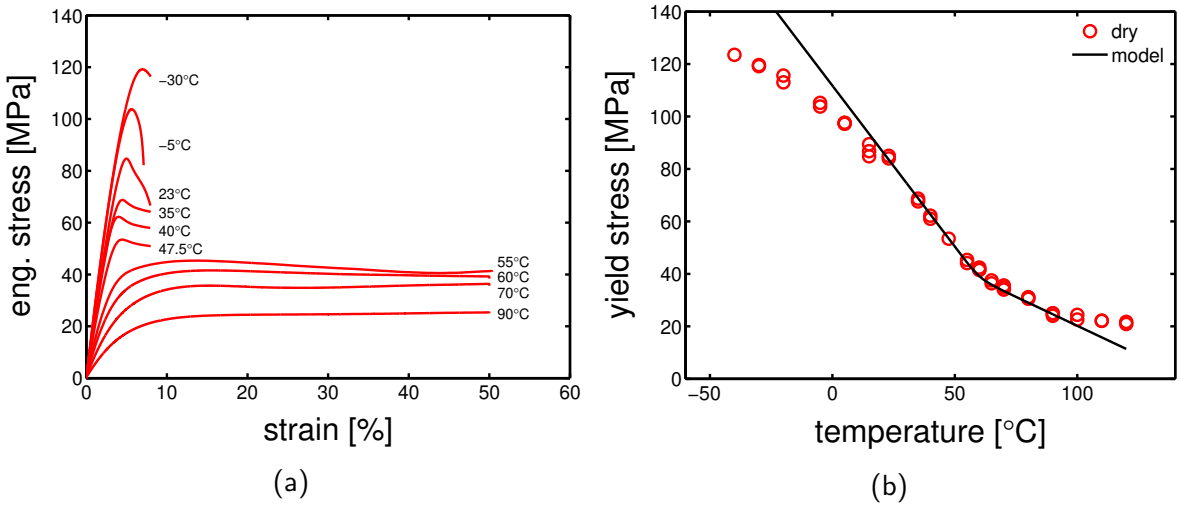

Figure 5: a) Examples of temperature-dependence of stress-strain response at the dry state and strain rate of $10^{-2}\ s^{-1}$; b) yield stress as a function of testing temperature.

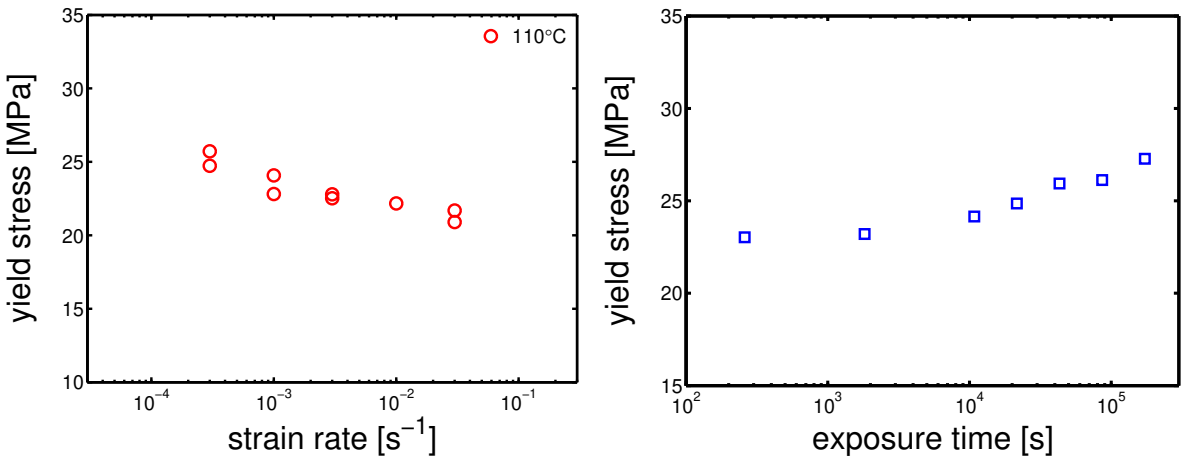

(a) (b)

Figure 6: a) Yield kinetics for dry samples testes at 110°C and different strain rates. This plot shows the result of the structure evolution which takes place during testing. b) Yield stress as a function of exposure time at 110°C prior to test.

4.2 Influence of humidity

As explained in section 1, the conditioning environment (i.e. temperature and humidity) has a crucial influence on the glass transition of PA6. Thus, the samples were exposed to four different moist environment (RH35%, RH50%, RH75% and under water) for a certain time up to saturation. The absorbed water fraction was calculated by the following:

$$H_2O\% = (\frac{W_i - W_0}{W_0}) \times 100 \tag{7}$$

where W_0 is the weight of the sample before conditioning and W_i is the weight at the time t_i. In figure 7a, an example of water absorption kinetics is shown. As shown, after a certain time, the absorbed water fraction reaches a plateau, which is considered as saturation level.

an investigation of the moisture-induced glass transition depression was performed by DMTA. In figure 8a the phase angle ($\tan(\delta)$) of samples conditioned at different humidity is plotted as function of temperature. The maximum defines the glass transition temperature; as expected, the higher the relative humidity the lower the glass T_g. In figure 8b, the glass transition tem-

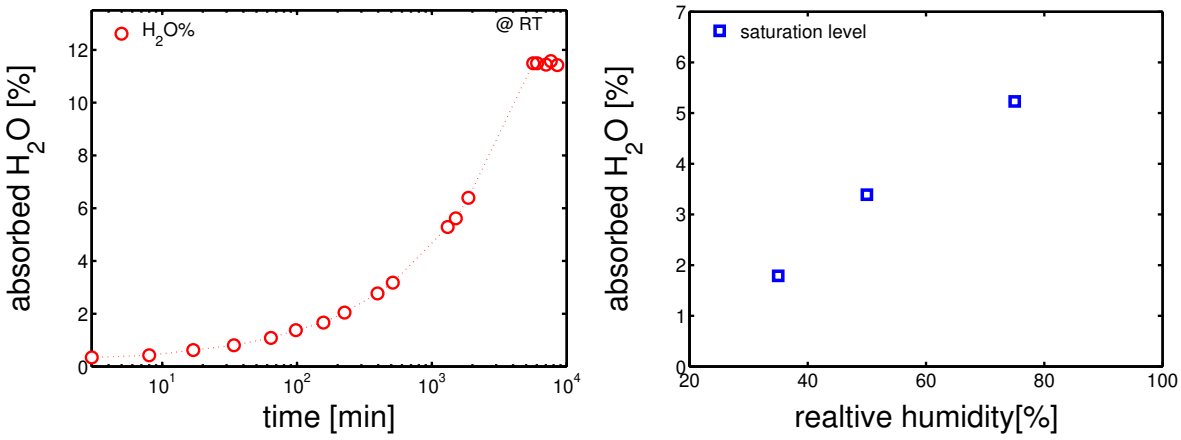

(a) (b)

Figure 7: (a) Example of water absorption kinetics, the absorbed water fraction is plotted as a function of time in the case of samples soaked in water. b) Saturation level as a function of relative humidity, conditioning at 23°C.

peratures obtained by DMTA, are plotted as a function of up-taken water fraction. T_g drops from about 60 °C for the dry sample to about -20°C for sample soaked in water. In table 2 the glass transition temperature are reported.

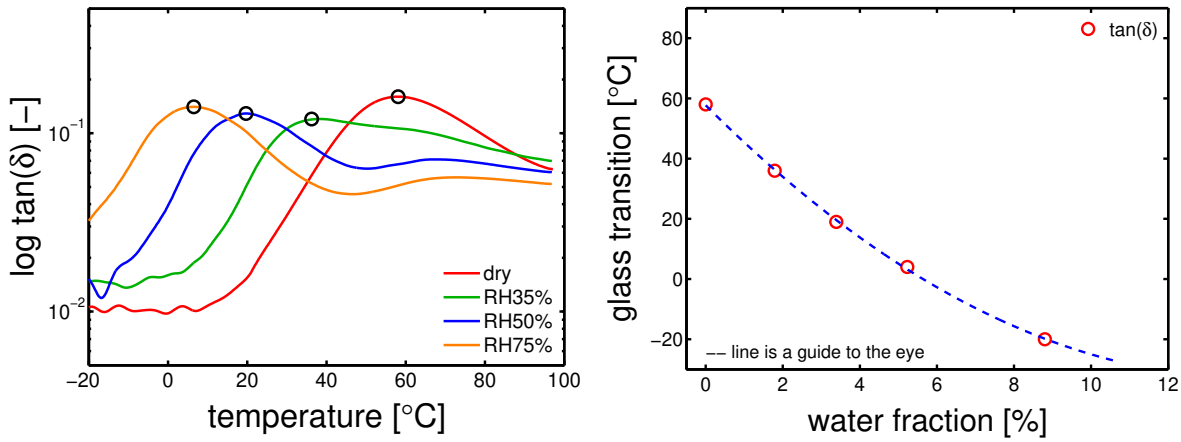

(a) (b)

Figure 8: (a) DMTA results, log tan(δ) as a function of temperature for samples conditioned at different humidity; markers are the T_g. (b) Glass transition temperature (obtained by DMTA) as function of the water fraction absorbed by the sample.

Table 2: Glass transition temperature after conditioning.

[°C]	dry	RH35%	RH50%	RH75%	water
T_g	58	36	19	4	-20

Because of the T_g depression due to hydration, crystallization can occur at room temperature during conditioning. In figure 9a the wide WAXD patterns are given for the four different relative humidity; figure 9b shows the crystalline fraction evolution as a function of relative humidity. Figure 9b shows the effect of hydration on crystallographic structures; as already mentioned, at dry condition the sample has a crystallinity of about 30% of solely γ-mesophase, upon hydration part of the gamma phase transform to α-phase till a value of about 8% α-phase and 23% γ-mesophase at 75%RH.

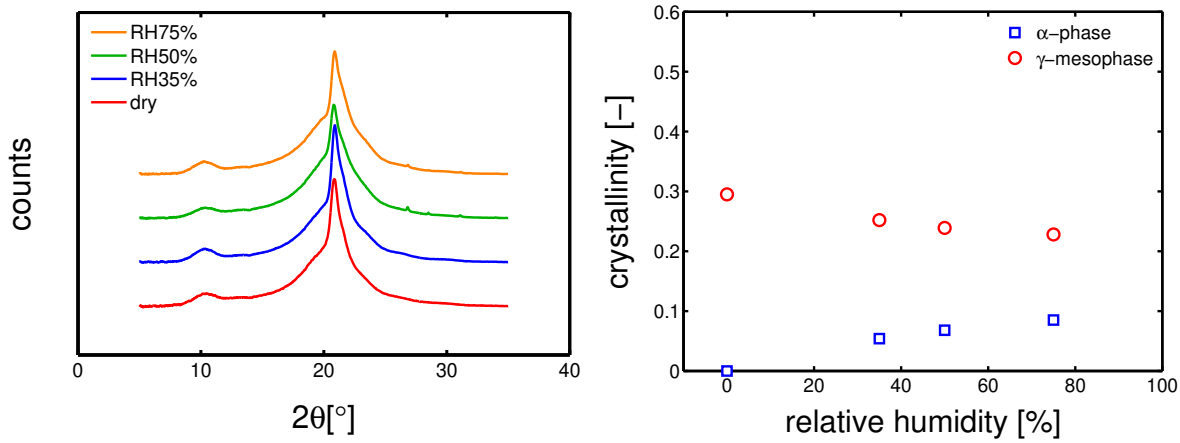

Figure 9: a) Wide angle x-ray diffraction patterns of samples conditioned at different relative humidity; b) crystalline fractions as a function of relative humidity.

Table 3: Crystallinity after conditioning.

[%]	dry	RH35%	RH50%	RH75%
γ	30	25	24	23
α	0	5	7	9

Next, the samples conditioned at different RH% are tested, an example is given in figure 10a; as mentioned, hydration lower the stress-strain response. Experiments were performed at several strain rates and relative humidity, in figure 10b the deformation kinetics for samples conditioned at different RH% is shown. In this case, the lines are the results of the Ree-Eyring equation but after a modification which includes the effect of relative humidity. The modification is based on one simple hypothesis: the enhancement of chain mobility due to an increase of temperature is comparable to the enhancement obtained by hydration. In order to quantify the effect of humidity, the drop of glass transition temperature is taken as reference; thus, the temperature in the equation 6 is replaced with an "apparent temperature" ($\tilde{T}$):

$$\widetilde{T} = T \; + \; (T_{g,dry} - T_{g,wet}) \tag{8}$$

where T is the actual testing temperature, $T_{g,dry}$ is the glass transition temperature at the dry state and $T_{g,wet}$ is the T_g after conditioning. A similar modification can be found in Söntjens *at al* [29], where the temperature is replaced by an equation which includes the change in T_g due different molecular weights in poly-D,L-lactide.

The equation 6 is re-written:

$$\sigma_y(\dot{\varepsilon}, \widetilde{T}) = \frac{k\widetilde{T}}{V_I^*} \; sinh^{-1}\left(\frac{\dot{\varepsilon}}{\dot{\varepsilon}_{0,I}} \; exp\left(\frac{\Delta U_I}{R\widetilde{T}}\right)\right) + \frac{k\widetilde{T}}{V_{II}^*} \; sinh^{-1}\left(\frac{\dot{\varepsilon}}{\dot{\varepsilon}_{0,II}} \; exp\left(\frac{\Delta U_{II}}{R\widetilde{T}}\right)\right) \tag{9}$$

As shown in figure 10b, this modification results in a good prediction of yield stress, the same parameters reported in table 1 were employed.

4.3 Long-term failure

After a wide investigation of deformation kinetics with experiments at constant strain rate, creep tests (constant load) are employed to study the influence of hydration on the time-to-failure. In figure 11a, two examples of creep test are shown; the annotations help to understand the definition of plastic flow rate ($\dot{\varepsilon}_{pl}$) and critical strain (ε_{cr}). Figure 11b reports the $\dot{\varepsilon}_{pl}$ as a

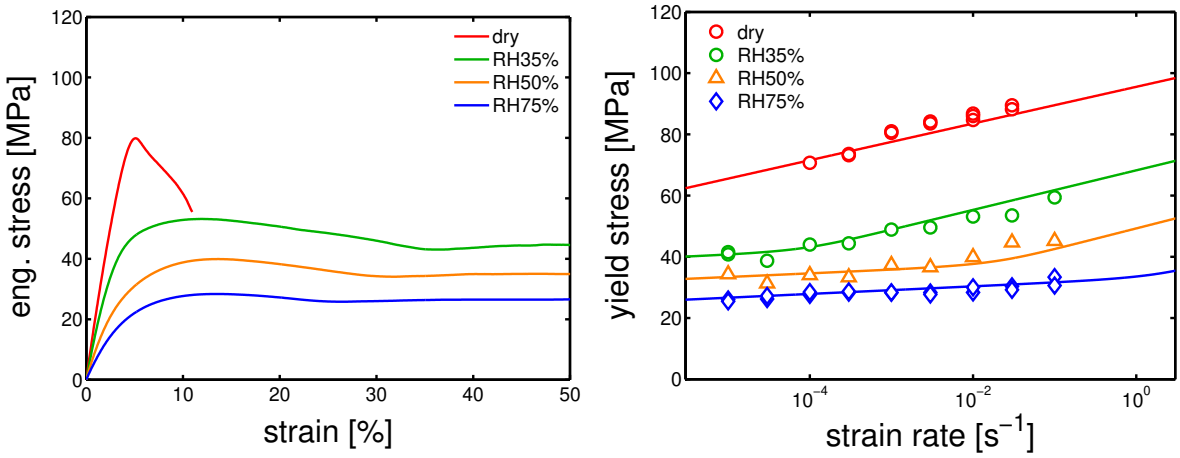

(a) (b)

Figure 10: a) Stress-strain response and b) yield kinetics of samples conditioned at different RH%.

function of time-to-failure for creep tests performed at several applied load and three different relative humidities. As explained in section 2, the bi-logarithmic plot of $\dot{\varepsilon}_{pl}$ versus t_f shows a slope of -1.

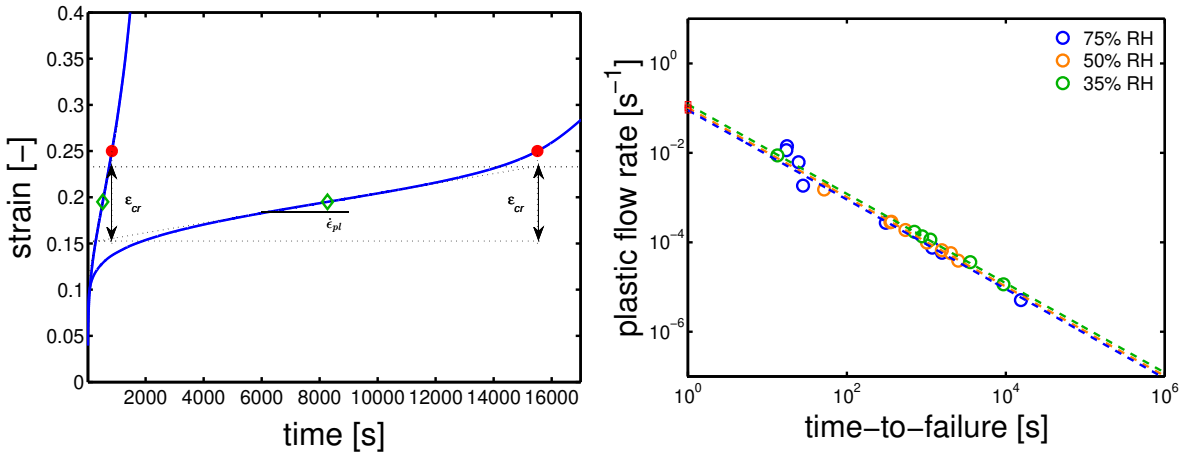

(a) (b)

Figure 11: a) Example of creep test at constant applied load, it shows the definition of $\dot{\varepsilon}_{pl}$, ε_{cr} and t_f. b) Plastic flow rate as a function of time to failure for samples conditioned at different relative humidity.

Finally, in figure 12a and 12b the applied stress is plot as a function of plastic flow rate (a) and time-to-failure (b), where the lines are results of the equations 9 and 3 respectively. Both the predictions (lines) describe well the experimental results (markers).

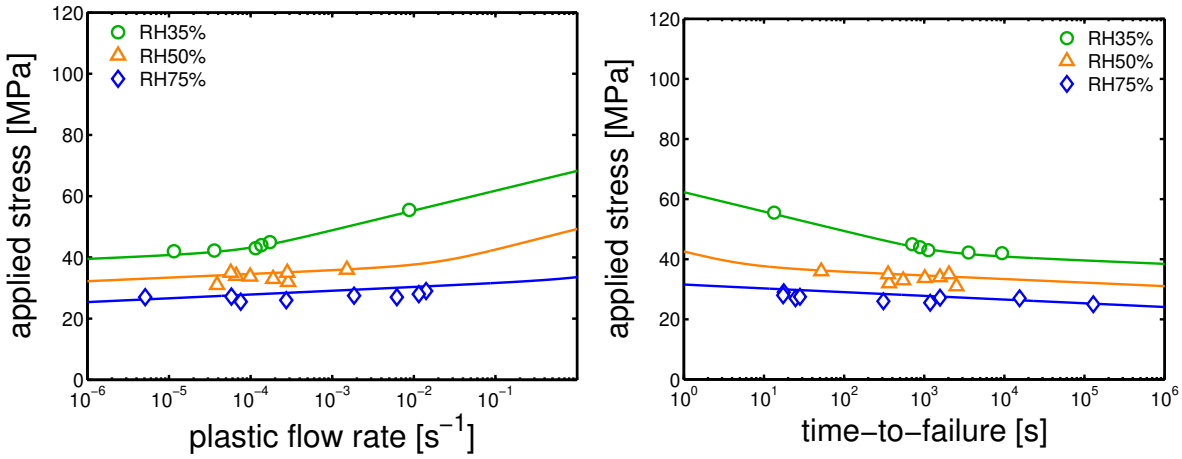

Figure 12: Applied stress as a function of a) plastic flow rate and b) time-to-failure for samples conditioned at different relative humidity.

4.4 Deformation mechanisms

As already mentioned, experimental evidences suggest that the deformation takes place through (at least) two different mechanisms which act in parallel. These two are strain rate- temperature-activated processes and they are additive to each other, therefore by varying the temperature (or relative humidity) and strain rate it is possible to observe deformation governed by processes I or I+II. These two mechanism are usually associated to an intra-lamellar (process I) and inter-lamellar deformation (process II). More in details, it is proposed that:

- Process I (intra-lamellar) is active below melting temperature (T_m), it is governed by plastic deformation of lamella via crystallographic slip, which is facilitated by the movement of screw dislocation present in the crystals. Thus, an increase of crystal mobility

due to temperature and/or an enhancement of mobility in the amorphous regions due to hydration improves the movement of these imperfections, facilitating the deformation.

- Process II (inter-lamellar) it is related to the deformation of the inter-lamellar amorphous region. The depression of glass transition and/or an increase of temperature lead to higher mobility in the amorphous regions, which results in an easier deformation.

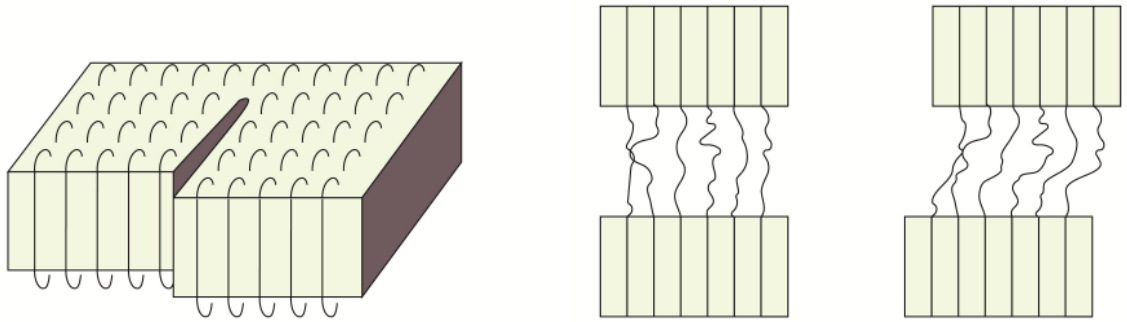

(a) (b)

Figure 13: a) Screw dislocation (schematic), b) mobilization of the inter-lamellar amorphous region (schematic).

5 Conclusions

In this study, the effect of temperature and relative humidity on the mechanical properties of melt processed polyamide 6 was investigated. PA6 shows a strong dependency on temperature, in the investigated range (from -40°C to 120°C) yield stress varies from about 125 MPa to 20 MPa at a strain rate of $10^{-2}\ s^{-1}$. Hydration strongly lowers the glass transition temperature, this affect substantially the mechanical properties. The pre-existing Eyring equation was modified in order to include the effect of humidity (T_g depression), the temperature was replaced by the "apparent temperature". After this modification, the Eyring equation is therefore suitable to predict the deformation kinetics of polyamide 6 at different temperatures and relative humidity. Moreover, by the introduction of the critical strain, the predictions made for the deformation kinetics (tensile test - constant plastic strain rate) can be translated also to predictions of time-to-failure (creep test - constant load) for different relative humidity.

References

[1] D.R. Holmes, C.W. Bunn, D.J. Smith, and Imperial Chemical. The Crystal Structure of Polycaproamide : Nylon 6. *J. Polym. Sci.*, 17:159–177, 1955.

[2] R. Puffr, J Bebenda, J. Šebenda, J. Bebenda, and J. Šebenda. On the Structure and Properties of Polyamides. XXVII. The Mechanism of Water Sorption in Polyamides. *J. Polym. Sci. Part C Polym. Symp.*, 16(1):79–93, 2007.

[3] N.S. Murthy, M. Stamm, J.P. Sibilia, and S. Krimm. Structural changes accompanying hydration in nylon 6. *Macromolecules*, 22(3):1261–1267, 1989.

[4] N.S. Murthy. Hydrogen bonding, mobility, and structural transitions in aliphatic polyamides. *Journal of Polymer Science, Part B: Polymer Physics*, 44(13):1763–1782, 2006.

[5] T.S. Ellis. Moisture-induced plasticization of amorphous polyamides and their blends. *Journal of Applied Polymer Science*, 36(3):451–466, 1988.

[6] I. Boukal. Effect of water on the mechanism of deformation of nylon 6. *J. Appl. Polym. Sci.*, 11(8):1483–1494, 1967.

[7] N. Jia, H.A. Fraenkel, and V.A. Kagan. Effects of Moisture Conditioning Methods on Mechanical Properties of Injection Molded Nylon 6. *J. Reinf. Plast. Compos.*, 23(7):729–737, 2004.

[8] V. Miri, O. Persyn, J.-M. Lefebvre, and R. Seguela. Effect of water absorption on the plastic deformation behavior of nylon 6. *Eur. Polym. J.*, 45(3):757–762, 2009.

[9] H.K. Reimschuessel and Allied Chemical. Relationships on the effect of water on glass transition temperature and young s modulus of nylon 6. *J. Polym. Sci. Polym. chemisrty Ed.*, 16(6):1229–1236, 1978.

[10] N.S Murthy, Z.-G Wang, M.K Akkapeddi, and B.S Hsiao. Isothermal crystallization kinetics of nylon 6, blends and copolymers using simultaneous small and wide-angle X-ray measurements. *Polymer (Guildf).*, 43(18):4905–4913, 2002.

[11] D. Cavallo, L. Gardella, G.C. Alfonso, G. Portale, L. Balzano, and R. Androsch. Effect of cooling rate on the crystal/mesophase polymorphism of polyamide 6. *Colloid and Polymer Science*, 289(9):1073–1079, 2011.

[12] A. Ramkumar and R. Gnanamoorthy. Axial fatigue behaviour of polyamide-6 and polyamide-6 nanocomposites at room temperature. *Composites Science and Technology*, 68(1516):3401 – 3405, 2008.

[13] Simon C. Bellemare, Martin N. Bureau, Johanne Denault, and J. Ivan Dickson. Fatigue crack initiation and propagation in polyamide-6 and in polyamide-6 nanocomposites. *Polymer Composites*, 25(4):433–441, 2004.

[14] M.D. Skibo, R.W. Hertzberg, J.A. Manson, and S.L. Kim. On the generality of discontinuous fatigue crack growth in glassy polymers. *Journal of Materials Science*, 12(3):531–542, 1977.

[15] F. Ramsteiner and T. Armbrust. Fatigue crack growth in polymers. *Polymer Testing*, 20(3):321 – 327, 2001.

[16] R.W. Hertzberg and J. A. Manson. *Fatigue of engineering plastics*. Academic press, 1980.

[17] P.E Tomlins, B.E Read, and G.D Dean. The effect of temperature on creep and physical ageing of poly(vinyl chloride). *Polymer*, 35(20):4376 – 4381, 1994.

[18] N. Verheulpen-Heymans and J.C. Bauwens. Effect of stress and temperature on dry craze growth kinetics during low-stress creep of polycarbonate. *Journal of Materials Science*, 11(1):7–16, 1976.

[19] C. Bauwens-Crowet, J.-M. Ots, and J.-C. Bauwens. The strain-rate and temperature dependence of yield of polycarbonate in tension, tensile creep and impact tests. *Journal of Materials Science*, 9(7):1197–1201, 1974.

[20] H. Eyring. Viscosity, plasticity, and diffusion as examples of absolute reaction rates. *The Journal of Chemical Physics*, 4(4):283–291, 1936.

[21] M.J.W. Kanters, K. Remerie, and L.E. Govaert. A new protocol for accelerated screening of long-term plasticity-controlled failure of polyethylene pipe grades. *Polymer Engineering and Science*, 56(6):676–688, 2016.

[22] M.C. Boyce, D.M. Parks, and A.S. Argon. Large inelastic deformation of glassy polymers. part i: rate dependent constitutive model. *Mechanics of Materials*, 7(1):15 – 33, 1988.

[23] O.D. Sherby and J.E. Dorn. Anelastic creep of polymethyl methacrylate. *Journal of the Mechanics and Physics of Solids*, 6(2):145 – 162, 1958.

[24] J.A Roetling. Yield stress behaviour of isotactic polypropylene. *Polymer*, 7(7):303 – 306, 1966.

[25] C. Bauwens-Crowet, J. C. Bauwens, and G. Homs. Tensile yield-stress behavior of glassy polymers. *Journal of Polymer Science Part A-2: Polymer Physics*, 7(4):735–742, 1969.

[26] T.B. Van Erp, C.T. Reynolds, T. Peijs, J.A.W. Van Dommelen, and L.E. Govaert. Prediction of yield and long-term failure of oriented polypropylene: Kinetics and anisotropy. *Journal of Polymer Science, Part B: Polymer Physics*, 47(20):2026–2035, 2009.

[27] H. Kawai, T. Hashimoto, S. Suehiro, and Ken-Ich F. Dynamic x-ray diffraction studies of spherulitic poly-alpha-olefins in relation to the assignments of alpha and beta mechanical dispersions. *Polymer Engineering & Science*, 24(5):361–372, 1984.

[28] R. Hiss, S. Hobeika, C. Lynn, and G. Strobl. Network stretching, slip processes, and fragmentation of crystallites during uniaxial drawing of polyethylene and related copolymers. a comparative study. *Macromolecules*, 32(13):4390–4403, 1999.

[29] S.H.M. Söntjens, T.A.P. Engels, T.H. Smit, and L.E. Govaert. Time-dependent failure of amorphous poly-d,l-lactide: Influence of molecular weight. *Journal of the Mechanical Behavior of Biomedical Materials*, 13:69 – 77, 2012.

5.1 Appendix A

In order to explain the partial mismatch between prediction and results of figure 5a, compression tests were performed with strain rate $10^{-2}\ s^{-1}$ (the same of tensile test) in a range of temperatures from -40°C to 120°C. The experiments were performed on cylindrical sample of about 3 mm height and 3 mm diameter; in order to decrease the friction between sample and the compression tool, they the samples were wrapped in PTFE tape and before every experiment, a layer of PTFE spray was sprayed on the testing surfaces.

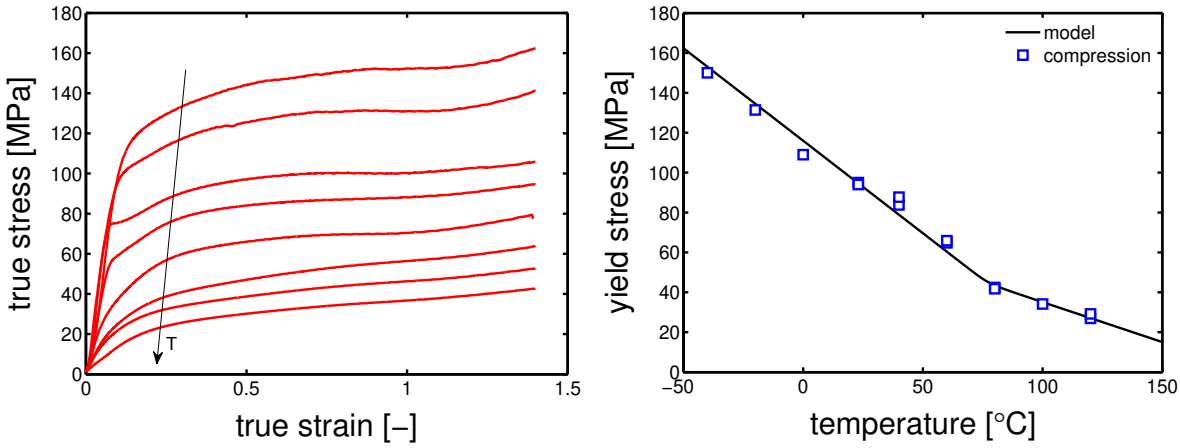

(a) (b)

Figure 14: a) True stress versus true strain of.

Figure 14b proves that the partial mismatch between prediction and experimental results shown in figure 5a is exclusively due to a geometric effect which unavoidable unless by changing the testing technique.